Pion condensation versus color superconductivity, speed of sound, and charge neutrality effects in the quark-meson diquark model

Jens O. Andersen* and Mathias P. Nødtvedt†

Department of Physics, Faculty of Natural Sciences, NTNU, Norwegian University of Science and Technology, Høgskoleringen 5, N-7491 Trondheim, Norway

(Received 28 March 2025; accepted 28 August 2025; published 23 January 2026)

We employ the two-flavor quark-meson diquark model as a low-energy model for QCD at nonzero quark and isospin chemical potentials μ and μ_I, and at zero temperature. We map out the phase diagram in the μ–μ_I plane, which has four phases: a vacuum phase, a phase with condensed charged pions/Cooper pairs of u and $\bar{d}$ quarks, a normal quark matter (NQM) phase, and a color superconducting phase (2SC phase). The global symmetry breaking $SU(3)_c \to SU(2)_c$ in the 2SC phase gives rise to a number of Nambu-Goldstone bosons. We classify them and briefly discuss their properties. We calculate the speed of sound c_s in the two special cases, finite μ_I and $\mu = 0$, and finite μ and $\mu_I = 0$. In both cases, the speed of sound exhibits a maximum and approaches the conformal limit from above as the density increases. For nonzero isospin μ_I, this behavior is in agreement with the speed of sound obtained from lattice simulations. In the 2SC phase, the behavior is qualitatively the same if we impose local charge neutrality. Finally, we discuss the possibility of having a mixed phase of negatively charged NQM and positively charged 2SC matter with global color charge neutrality imposed on the latter.

DOI: 10.1103/vwbc-n1rt

I. INTRODUCTION

QCD in extreme conditions has been of interest for decades due to its relevance to the early Universe, heavy-ion collisions, and compact stars [1–3]. The QCD phase diagram, which conventionally is drawn in the μ_B–T plane, turns out to be very rich, with a number of phases. It becomes even more complicated if we allow an independent chemical potential for each quark flavor f instead of a common quark chemical potential μ. For two quark flavors, we can use μ_u and μ_d or equivalently use the isospin chemical potential $\mu_I = \mu_u - \mu_d$ and the baryon chemical potential $\mu_B = 3\mu$. For three flavors, we add a μ_S axis, where S is strangeness, and $\mu_S = \frac{1}{2}(\mu_u + \mu_d - 2\mu_s)$. Consider the phase diagram in the μ_B–μ_I plane. Moving along the μ_I axis, the QCD is in the vacuum phase until the isospin chemical potential reaches the critical value $\mu_I^c = m_\pi$, which marks the onset of charge pion condensation [4]. For sufficiently small values of μ_I, the pion-condensed phase can be described in a model-independent way using chiral perturbation theory [5,6]. For very large values of μ_I, quarks and gluons are the relevant degrees of freedom, and if the density is sufficiently high, one can use perturbative QCD (pQCD). In pQCD, one-gluon exchange gives rise to an attractive quark-quark interaction channel. According to Bardeen-Cooper-Schrieffer (BCS) theory for superconductivity, any attractive interaction renders the Fermi sphere unstable, and Cooper pairs are formed. Since $\mu_u = -\mu_d$, these pairs consist of u quarks and $\bar{d}$ antiquarks or vice versa depending on the sign of μ_I. Thus, QCD at very large isospin chemical potential is a color superconductor. The diquark condensate or the gap has the same quantum numbers as those of the pion condensate that exists for low values of μ_I, so one expects a crossover from a pion condensate to a color-superconducting state (BEC/BCS crossover) as one increases μ_I [4]. A nice feature of QCD at nonzero μ_I, but $\mu_B = 0$ is the absence of the sign problem and the possibility to perform lattice simulations. It is then possible to compare lattice QCD [7–9] with model-independent predictions for small μ_I using chiral perturbation theory [4,10], and perturbative QCD for large μ_I.

The situation is similar at large baryon chemical potential, where perturbative QCD can be applied. Again, there is an attractive channel that involves one-gluon exchange. For sufficiently large values of μ_B, all three quark flavors can be taken massless, and they participate in the pairing on an equal footing as do the quarks of different colors. The resulting ground state is referred to as the color-flavor-locked (CFL) phase of QCD, whose existence at asymptotically large baryon chemical potential is one of the few

*Contact author: jens.andersen@ntnu.no
†Contact author: mathias.p.nodtvedt@ntnu.no

rigorous results in cold and dense QCD. Moving toward smaller values of μ_B, one can no longer ignore the mass of the s quark. The finite value of m_s places stress on pairs that contain an s quark. Eventually, it is energetically advantageous to break up such pairs, and one is left with a pairing pattern that involves the u and d quarks and two of the three colors. This phase is referred to as the 2SC phase.[1] Note, however, that the existence of the 2SC phase depends on the details of the models employed. For example, in the Nambu-Jona-Lasinio (NJL) model, there is a 2SC phase between the phase of normal quark matter (NQM) and the CFL phase if the couplings are small. For larger values of the couplings, the transition is from the CFL phase directly to normal quark matter [12–14].

The interest in QCD at finite quark chemical potentials and low temperature is mainly due to its applications to compact stars. Knowing the equation of state (EoS) allows us to calculate macroscopic quantities such as masses and radii of individual neutron stars, as well as tidal deformabilities in binary systems. The recent observations of compact stars of more than two solar masses put constraints on the EoS, and one of the main questions is whether the most massive stars have a quark core surrounded by ordinary nuclear matter. The quest for a phase transition in dense QCD has been hampered by the inapplicability of lattice QCD at finite μ_B due to the sign problem. The sign problem forces one to use other methods. At very large values of the baryon chemical potential, perturbative QCD is applicable due to asymptotic freedom. In recent years, perturbative calculations have been pushed to order $\alpha_3^3\log\alpha_s$, where α_s is the strong coupling [15,16]. In Ref. [17], renormalization group methods have been used to improve the convergence of the perturbative series. For lower values of μ, where pQCD cannot be applied, one uses low-energy effective models that in some aspects resemble QCD. The NJL model is an example of a low-energy effective model that incorporates chiral symmetry breaking in the vacuum, but has no dynamical gauge fields. The local $SU(3)_c$ gauge symmetry is then replaced by the corresponding global symmetry.

The present work is a continuation of Ref. [18]. In that paper, we formulated the two-flavor quark-meson diquark (QMD) model as a renormalizable low-energy effective model for two-flavor QCD, with meson, quark, and diquark degrees of freedom. In this paper, we continue our study of the model and its properties, focusing on the phase diagram in the μ_I–μ plane, the speed of sound, and the effects of imposing neutrality for electric and color charge. Regarding the phase diagram, we will also use some results from Ref. [19]. In that paper, the thermodynamic potential Ω including a pion condensate at finite μ_I was calculated in the same approximation as used here. By comparing the pressure in the different phases (vacuum, normal quark matter, pion condensed phase, or 2SC phase) for a given pair (μ,μ_I), we can map out the phase diagram.

II. TWO-FLAVOR QMD MODEL

A. Lagrangian

The Minkowski Lagrangian for the two-flavor quark-meson diquark model is

$$\begin{aligned}\mathcal{L} &= \frac{1}{2}(\partial_\mu\sigma)(\partial^\mu\sigma)+\frac{1}{2}(\partial_\mu\pi_0)(\partial^\mu\pi_0)+(\partial_\mu+i\mu_I\delta_{\mu0})\pi^+(\partial^\mu-i\mu_I\delta^{\mu0})\pi^- -\frac{1}{2}m^2(\sigma^2+\vec{\pi}^2)-\frac{\lambda}{24}(\sigma^2+\vec{\pi}^2)^2\\ &\quad + h\sigma+(\partial_\mu+2i\mu_a\delta_{\mu0})\Delta_a^\dagger(\partial^\mu-2i\mu_a\delta^{\mu0})\Delta_a-m_\Delta^2\Delta_a^\dagger\Delta_a-\frac{\lambda_3}{12}(\sigma^2+\vec{\pi}^2)\Delta_a^\dagger\Delta_a-\frac{\lambda_\Delta}{6}(\Delta_a^\dagger\Delta_a)^2\\ &\quad +\bar{\psi}(i\partial\!\!\!/+\gamma^0\hat{\mu})\psi-g\bar{\psi}[\sigma+i\gamma^5\vec{\pi}\cdot\vec{\tau}]\psi+\frac{1}{2}g_\Delta\bar{\psi}_b^C\Delta_a\gamma^5\tau_2\epsilon_{abc}\psi_c+\frac{1}{2}g_\Delta\bar{\psi}_b\Delta_a^\dagger\gamma^5\tau_2\epsilon_{abc}\psi_c^C,\end{aligned} \tag{1}$$

where ψ is a flavor doublet and a color triplet in the fundamental representation

$$\psi=\begin{pmatrix}\psi_{ur}\\ \psi_{dr}\\ \psi_{ug}\\ \psi_{dg}\\ \psi_{ub}\\ \psi_{db}\end{pmatrix}. \tag{2}$$

Furthermore, ψ_c is the flavor doublet with color c

$$\psi_c=\begin{pmatrix}\psi_{uc}\\ \psi_{dc}\end{pmatrix}. \tag{3}$$

The field Δ_a is a composite diquark field, $\Delta_a\sim\bar{\psi}_b\gamma^5\tau_2\epsilon_{abc}\psi_c^C$, where $\psi^C=C\bar{\psi}^T$ and $C=i\gamma^2\gamma^0$ is the charge conjugation operator, which can be written as

$$\Delta=\begin{pmatrix}\Delta_1\\ \Delta_2\\ \Delta_3\end{pmatrix}. \tag{4}$$

The diquark field Δ transforms as a singlet under $SU(2)_L\times SU(2)_R$ and as an antitriplet under $SU(3)_c$. Furthermore, $\hat{\mu}$

[1] Before the breakup of Cooper pairs, the stress on them may be relieved by kaon condensation. The system is still in the CFL phase, but the condensation corresponds to a rotation of the order parameter [11].

is the quark chemical potential matrix, μ_I is the isospin chemical potential for electrically charged pions, and μ_a is the chemical potential for diquark a. The chemical potentials $\hat{\mu}$, μ_a, and μ_I are not independent, but can be expressed in terms of μ_B, μ_e, and μ_8, which are the chemical potentials for baryon number, electric charge Q_e, and color charge Q_8 (see Sec. II B). The symmetries of the Lagrangian in Eq. (1) were discussed in some detail in Ref. [18], here we simply state them. In the chiral limit, the global symmetries are $SU(2)_L \times SU(2)_R \times U(1)_B \times SU(3)_c$, while at the physical point, the global symmetry is $SU(2)_V \times U(1)_B \times SU(3)_c$. The diquark condensate $\Delta_0 = \langle \Delta_3 \rangle$ in the 2SC phase breaks $SU(3)_c$ to $SU(2)_c$. The $U(1)_B$ symmetry in the vacuum, which is generated by $B = \frac{1}{3}\mathrm{diag}(1,1,1)$ is modified in the medium, $\tilde{B} = B - \frac{2}{\sqrt{3}} T_8 = \mathrm{diag}_c(0,0,1)$, where T_a are the generators of $SU(3)$. In the 2SC phase, only the blue quasiparticles carry a nonzero $\tilde{B}$ charge [20]. Similarly, there is an unbroken modified $U(1)$ symmetry generated by $Q' = Q - \frac{1}{\sqrt{3}} T_8$, where $Q = \mathrm{diag}(\frac{2}{3}, -\frac{1}{3})$ is the generator of the electromagnetic $U(1)$ symmetry. In the QMD model, this symmetry is global, whereas in QCD it is local. The gauge boson associated with this symmetry is then the in-medium photon. In the condensed phase of the pion, the condensate ρ_0 breaks the symmetry $U(1)_{I_3}$ associated with the third component of the isospin, that is, the subgroup of $SU(2)_V$. The $U(1)$ electromagnetic symmetry is also broken since $I_3 = Q + \frac{1}{6}\mathbb{1}$.

The Lagrangian has a number of masses and couplings. They can be grouped according to which sector they belong. The masses and couplings are all running parameters that depend on the renormalization scale Λ and each of them satisfies a renormalization group equation. These equations and their solutions, i.e., the running parameters were derived in Ref. [18]. The running masses and couplings can be used to obtain an RG-improved effective potential.

B. Chemical potentials and neutrality conditions

According to Noether's theorem, there is one conserved charge for each continuous symmetry of a system. In principle, one can introduce an independent chemical potential μ_i for each conserved charge Q_i. The corresponding number density is denoted by n_{Q_i}. However, this can only be done if the charges commute. In other words, we can introduce a maximum of N independent chemical potentials corresponding to the maximum number N of commuting charges of the system. In the present case, these are the baryon chemical potential μ_B, the chemical potential for electric charge μ_e, and the chemical potentials for the color charges Q_3 and Q_8, μ_3, and μ_8. The pairing of quarks in the 2SC phase gives rise to a nonzero color charge Q_8 in the ground state, while $Q_3 = 0$. Therefore, it is sufficient to introduce μ_8. This is in contrast to the CFL phase of three-flavor QCD, where the ground state completely breaks the $SU(3)_c$ symmetry. For this reason, both μ_3 and μ_8 must be introduced in order to impose color charge neutrality.

The quark chemical potential matrix can be expressed in terms of μ_B, μ_e, and μ_8 as

$$\mu_{ij,ab} = \left(\frac{1}{3}\mu_B \delta_{ij} - \mu_e Q_{ij}\right)\delta_{ab} + \frac{2}{\sqrt{3}}\mu_8 \delta_{ij} (T_8)_{ab}, \quad (5)$$

where i, j are flavor indices and a, b are color indices, and Q_{ij} are the matrix elements of the matrix $Q = \mathrm{diag}(\frac{2}{3}, -\frac{1}{3})$. The expressions for the different quark chemical potentials follow from Eq. (5) as

$$\mu_{ur} = \mu_{ug} = \mu - \frac{2}{3}\mu_e + \frac{1}{3}\mu_8, \quad (6)$$

$$\mu_{dr} = \mu_{dg} = \mu + \frac{1}{3}\mu_e + \frac{1}{3}\mu_8, \quad (7)$$

$$\mu_{ub} = \mu - \frac{2}{3}\mu_e - \frac{2}{3}\mu_8, \quad (8)$$

$$\mu_{db} = \mu + \frac{1}{3}\mu_e - \frac{2}{3}\mu_8, \quad (9)$$

where $\mu = \frac{1}{3}\mu_B$ is the common quark chemical potential. The number densities are given by

$$n_B = -\frac{\partial \Omega}{\partial \mu_B}, \quad (10)$$

$$n_e = -\frac{\partial \Omega}{\partial \mu_e}, \quad (11)$$

$$n_8 = -\frac{\partial \Omega}{\partial \mu_8}, \quad (12)$$

where Ω is the thermodynamic potential. For arbitrary values of μ_B, μ_e, and μ_8, the electric charge density is nonzero, $n_e \neq 0$. However, a macroscopic chunk of quark matter must be electrically neutral, otherwise a huge energy price has to be paid due to the Coulomb interaction [20]. We therefore impose local electric charge neutrality on the system. The same remarks apply to the color charge Q_8 and we therefore impose the two constraints

$$\frac{\partial \Omega}{\partial \mu_e} = \frac{\partial \Omega}{\partial \mu_8} = 0, \quad (13)$$

which finally leaves us with a single independent chemical potential, e.g., μ_B. Electric charge neutrality is obtained by adding an electron background, which is achieved by adding the following term to the thermodynamic potential

$$\Omega_e = -\frac{4\mu_e^4}{3(4\pi)^2}, \quad (14)$$

TABLE I. Values of the four independent chemical potentials in normal quark matter and in the 2SC phase.

...	NQM	NQM ($m_s = 0$)	2SC	2SC ($m_s = 0$)
μ_B	Nonzero	Nonzero	Nonzero	Nonzero
μ_e	Nonzero	0	Nonzero	Nonzero
μ_3	0	0	0	0
μ_8	0	0	Nonzero	Nonzero

where we have taken the electrons to be massless. In nature, $U(1)_Q$ and $SU(3)_c$ are local symmetries, and the zeroth components of the gauge fields serve as chemical potentials. The values of these fields are dynamically driven to values that set the charges to zero [21,22]. In the quark-meson diquark model, the above-mentioned symmetries are global, and the chemical potentials must be introduced by hand. In normal quark matter, it is straightforward to derive that $\mu_8 = 0$ guarantees color charge neutrality. However, in two-flavor QCD, normal quark matter is electrically charged since the trace of the electric charge matrix is nonzero. This requires a nonzero μ_e and the presence of electrons. In the 2SC phase, electric and charge color neutrality is ensured by nonzero values of both μ_e and μ_8, as we shall see below. In Table I, we summarize the values of the independent chemical potentials for the two-flavor and three-flavor NQM and 2SC phases.

C. Quark spectrum and thermodynamic potential in the 2SC phase

We write the sigma σ and diquark field Δ_3 as a sum of their expectation values ϕ_0 and Δ_0, and quantum fluctuating fields. This is done by making the substitutions

$$\sigma \to \phi_0 + \sigma, \tag{15}$$

$$\Delta_3 \to \Delta_0 + \Delta_3, \tag{16}$$

in the Lagrangian. Choosing Δ_0 real, the resulting tree-level thermodynamic potential is

$$\Omega_0^{2\mathrm{SC}} = \frac{1}{2}m^2\phi_0^2 + (m_\Delta^2 - 4\bar{\mu}^2)\Delta_0^2 + \frac{\lambda}{24}\phi_0^4 + \frac{\lambda_3}{12}\phi_0^2\Delta_0^2 + \frac{\lambda_\Delta}{6}\Delta_0^4 - h\phi_0, \tag{17}$$

where $\bar{\mu}$ is defined in Eq. (25) below. The bilinear quark terms in the Lagrangian are

$$\mathcal{L}_{\mathrm{bilinear}} = \bar{\psi}[i\partial\!\!\!/ - g\phi_0 + \hat{\mu}\gamma^0]\psi + \frac{1}{2}g_\Delta\bar{\psi}_b^C\Delta_0\gamma^5\tau_2\epsilon_{3bc}\psi_c + \frac{1}{2}g_\Delta\bar{\psi}_b\Delta_0^\dagger\gamma^5\tau_2\epsilon_{3bc}\psi_c^C. \tag{18}$$

Using the Nambu-Gorkov basis, $\Psi = (\psi, \psi^C)^T$, we then find the following inverse quark propagator

$$D^{-1}(p) = \begin{pmatrix} p\!\!\!/ - g\phi_0 + \gamma^0\hat{\mu} & ig_\Delta\tau_2\lambda_2\gamma^5\Delta_0 \\ ig_\Delta\tau_2\lambda_2\gamma^5\Delta_0 & p\!\!\!/ - g\phi_0 - \gamma^0\hat{\mu} \end{pmatrix}. \tag{19}$$

The zeros of the determinant of $D^{-1}(p)$ give the fermion spectrum. We group the spectrum into the spectrum for the blue quarks

$$E_{ub}^{\pm} = E \pm \mu_{ub}, \tag{20}$$

$$E_{db}^{\pm} = E \pm \mu_{db}, \tag{21}$$

and the spectrum for the red and green quarks

$$E_{\Delta^{\pm}}^{\pm} = E_\Delta^{\pm} \pm \delta\mu, \tag{22}$$

where the energies and chemical potentials are defined as

$$E = \sqrt{p^2 + g^2\phi_0^2}, \tag{23}$$

$$E_\Delta^{\pm} = \sqrt{(E \pm \bar{\mu})^2 + g_\Delta^2\Delta_0^2}, \tag{24}$$

$$\bar{\mu} = \frac{1}{2}(\mu_{ur} + \mu_{dg}) = \frac{1}{2}(\mu_{ug} + \mu_{dr}) = \mu - \frac{1}{6}\mu_e + \frac{1}{3}\mu_8, \tag{25}$$

$$\delta\mu = \frac{1}{2}(\mu_{dg} - \mu_{ur}) = \frac{1}{2}(\mu_{dr} - \mu_{ug}) = \frac{1}{2}\mu_e. \tag{26}$$

The chemical potential $\delta\mu$ is referred to as the mismatch parameter since it measures the mismatch between the Fermi surfaces of the u and the d quarks, i.e., the quarks that form pairs. A large value $\delta\mu$ disfavors Cooper pairing as we shall see below. The ungapped quasiparticles Eqs. (20) and (21) are singlets under the unbroken $SU(2)_c$ symmetry, each with a degeneracy factor one. The quasiparticles in Eq. (22) form two doublets under the unbroken $SU(2)_c$ symmetry, each with a degeneracy factor of two. This gives a total of six quark and six antiquark quasiparticles. They become degenerate when the mismatch parameter vanishes. The doublet with energy $E_{\Delta^+}^-$ has a gap $g_\Delta\Delta_0 + \delta\mu$, while the doublet with energy $E_{\Delta^-}^-$ has a gap $g_\Delta\Delta_0 - \delta\mu$ as long as $\delta\mu < g_\Delta\Delta_0$. When $\delta\mu \geq g_\Delta\Delta_0$, this mode becomes gapless and the corresponding phase is referred to as the gapless 2SC phase [23].

We now turn to the thermodynamic potential Ω. We work in the approximation, where bosons are treated at tree level, whereas we include Gaussian fluctuations of the quarks. The one-loop contribution to the thermodynamic potential from the quarks is

$$\Omega_1^{\mathrm{2SC}} = -2\Lambda^{-2\epsilon}\int_p \{2E + T\log[1+e^{-\beta E_{ub}^{\pm}}] + T\log[1+e^{-\beta E_{db}^{\pm}}]\} - 4\Lambda^{-2\epsilon}\int_p \{E_\Delta^{\pm} + T\log[1+e^{-\beta E_{\Delta^{\pm}}^{\pm}}]\}, \tag{27}$$

which is added to the tree-level term Eq. (17). The integrals $\int_p$ are defined in $d = 3-2\epsilon$ dimensions as

$$\int_p = \left(\frac{e^{\gamma_E}\Lambda^2}{4\pi}\right)^{\epsilon}\int\frac{d^d p}{(2\pi)^d}, \tag{28}$$

where Λ is the renormalization scale associated with the $\overline{\mathrm{MS}}$ scheme. The final result for the thermodynamic potential at $T=0$, including quark loops, was derived in Ref. [18] and reads

$$\begin{aligned}
\Omega_{0+1}^{\mathrm{2SC}} = {} & \frac{3}{4}m_\pi^2 f_\pi^2\left\{1 - \frac{12m_q^2}{(4\pi)^2 f_\pi^2}m_\pi^2 F'(m_\pi^2)\right\}\frac{\phi_0^2}{f_\pi^2} + \frac{2m_q^4}{(4\pi)^2}\left(\frac{9}{2} + \log\frac{m_q^2}{g_0^2\phi_0^2} + 2\log\frac{m_q^2}{g_0^2\phi_0^2 + g_{\Delta,0}^2\Delta_0^2}\right)\frac{\phi_0^4}{f_\pi^4} \\
& - \frac{1}{4}m_\sigma^2 f_\pi^2\left\{1 + \frac{12m_q^2}{(4\pi)^2 f_\pi^2}\left[\left(1 - \frac{4m_q^2}{m_\sigma^2}\right)F(m_\sigma^2) + \frac{4m_q^2}{m_\sigma^2} - F(m_\pi^2) - m_\pi^2 F'(m_\pi^2)\right]\right\}\frac{\phi_0^2}{f_\pi^2} \\
& + \frac{1}{8}m_\sigma^2 f_\pi^2\left\{1 + \frac{12m_q^2}{(4\pi)^2 f_\pi^2}\left[\left(1 - \frac{4m_q^2}{m_\sigma^2}\right)F(m_\sigma^2) - F(m_\pi^2) - m_\pi^2 F'(m_\pi^2)\right]\right\}\frac{\phi_0^4}{f_\pi^4} \\
& - \frac{1}{8}m_\pi^2 f_\pi^2\left\{1 - \frac{12m_q^2}{(4\pi)^2 f_\pi^2}m_\pi^2 F'(m_\pi^2)\right\}\frac{\phi_0^4}{f_\pi^4} - m_\pi^2 f_\pi^2\left\{1 - \frac{12m_q^2}{(4\pi)^2 f_\pi^2}m_\pi^2 F'(m_\pi^2)\right\}\frac{\phi_0}{f_\pi} \\
& + \left\{m_{\Delta,0}^2 - 4\bar{\mu}^2\left[1 + \frac{4g_{\Delta,0}^2}{(4\pi)^2}\left(\log\frac{m_q^2}{g_0^2\phi_0^2 + g_{\Delta,0}^2\Delta_0^2} - F(m_\pi^2) - m_\pi^2 F'(m_\pi^2)\right)\right]\right\}\Delta_0^2 \\
& + \frac{\lambda_{3,0}}{12}\phi_0^2\Delta_0^2 + \frac{\lambda_{\Delta,0}}{6}\Delta_0^4 + \frac{12g_0^2 g_{\Delta,0}^2}{(4\pi)^2}\phi_0^2\Delta_0^2 + \frac{6g_{\Delta,0}^4}{(4\pi)^2}\Delta_0^4 \\
& + \frac{4g_{\Delta,0}^4}{(4\pi)^2}\left\{\log\frac{m_q^2}{g_0^2\phi_0^2 + g_{\Delta,0}^2\Delta_0^2} - F(m_\pi^2) - m_\pi^2 F'(m_\pi^2)\right\}\Delta_0^4 \\
& + \frac{4g_0^2 g_{\Delta,0}^2}{(4\pi)^2}\left\{\log\frac{m_q^2}{g_0^2\phi_0^2 + g_{\Delta,0}^2\Delta_0^2} - F(m_\pi^2) - m_\pi^2 F'(m_\pi^2)\right\}\phi_0^2\Delta_0^2 + \Omega_1^{\mathrm{2SC,fin}} + \Omega_1^{\mathrm{2SC},\mu},
\end{aligned} \tag{29}$$

where $g_{\Delta,0}^2$ and Δ_0^2 are the running coupling and field $g_{\Delta,\overline{\mathrm{MS}}}^2$ and $\Delta_{\overline{\mathrm{MS}}}^2$ evaluated at a reference scale, but the product $g_{\Delta,\overline{\mathrm{MS}}}^2\Delta_{\overline{\mathrm{MS}}}^2$ is scale invariant. The same remark applies to g_0^2 and ϕ_0^2. Moreover, the function $F(p^2) = 2 - 2q\arctan(\frac{1}{q})$ with $q = \sqrt{\frac{4m_q^2}{p^2} - 1}$, and

$$\Omega_1^{\mathrm{2SC,fin}} = -4\Lambda^{-2\epsilon}\int_p\left[E_\Delta^{\pm} - 2\sqrt{p^2 + g^2\phi_0^2 + g_\Delta^2\Delta_0^2} - \frac{\bar{\mu}^2 g_\Delta^2\Delta_0^2}{(p^2 + g^2\phi_0^2 + g_\Delta^2\Delta_0^2)^{\frac{3}{2}}}\right], \tag{30}$$

$$\Omega_1^{\mathrm{2SC},\mu} = 2\Lambda^{-2\epsilon}\int_p[(E \mp \mu_{ub})\theta(\pm\mu_{ub} - E) + (E \mp \mu_{db})\theta(\pm\mu_{db} - E) + 2(E_\Delta^{\pm} \mp \delta\mu)\theta(\pm\delta\mu - E_\Delta^{\pm})]. \tag{31}$$

Note that the integrals in Eqs. (30) and (31) are finite in $d=3$.

D. Nambu-Goldstone bosons in the 2SC phase

The formation of Cooper pairs and the resulting nonzero gap Δ_0 in the 2SC phase break the $SU(3)_c$ symmetry down to $SU(2)_c$. In QCD with dynamical gluons, there is no breaking of the local $SU(3)_c$ symmetry, however, and the gap Δ_0 is a gauge-variant quantity. Only the magnitude $|\Delta_0|$ is gauge invariant. Instead of a number of Nambu-Goldstone (NG) modes in the physical spectrum, the Higgs mechanism leads to five massive gluons, one for each broken generator [24]. In the QMD model, the $SU(3)_c$ symmetry is global and its breaking to $SU(2)_c$ should naively lead to five massless excitations, or NG bosons, corresponding to the five broken generators,[2] naively, since it is only in Lorentz-invariant theories that Goldstone's theorem guarantees that the number of massless excitations equals the number of broken generators. Starting with the paper by Chadha and Nielsen [27], there has been significant progress in the classification of NG bosons and their properties; see, e.g., [28–31], and [32] for a comprehensive review.

The complex antitriplet Δ_a can be parametrized in terms of six real fields. In order to simplify the discussion and obtain analytical results, we set $\phi_0 = 0$ in the remainder of this section. There is no loss of generality since the symmetry-breaking pattern in the diquark sector remains the same, $SU(3)_c \to SU(2)_c$. Writing $\Delta_3 = \Delta_0 + \frac{1}{\sqrt{2}}(\phi_1 + i\phi_2)$ and using a common quark chemical potential μ, the relevant terms up to quadratic order are

$$\begin{aligned}\mathcal{L}_{\rm quad}^{\rm bosons} =& (\partial_\mu + 2i\delta_{\mu0}\mu)\Delta_1^\dagger(\partial_\mu - 2i\delta_{\mu0}\mu)\Delta_1 - \left(m_\Delta^2 + \frac{\lambda_\Delta}{3}\Delta_0^2\right)\Delta_1^\dagger\Delta_1 + (\partial_\mu + 2i\delta_{\mu0}\mu)\Delta_2^\dagger(\partial_\mu - 2i\delta_{\mu0}\mu)\Delta_2 \\ &- \left(m_\Delta^2 + \frac{\lambda_\Delta}{3}\Delta_0^2\right)\Delta_2^\dagger\Delta_2 + \frac{1}{2}(\partial_\mu\phi_1)(\partial^\mu\phi_1) - \frac{1}{2}(m_\Delta^2 - 4\mu^2 + \lambda_\Delta\Delta_0^2)\phi_1^2 \\ &+ \frac{1}{2}(\partial_\mu\phi_2)(\partial^\mu\phi_2) - \frac{1}{2}\left(m_\Delta^2 - 4\mu^2 + \frac{\lambda_\Delta}{3}\Delta_0^2\right)\phi_2^2 + 2\mu(\partial_0\phi_1\phi_2 - \partial_0\phi_2\phi_1). \end{aligned} \tag{32}$$

The spectrum is found by calculating the zeros of the determinant of the propagator in the usual way. Note that we need to evaluate the expectation value of the diquark field, Δ_0, at the minimum (on shell) of the tree-level thermodynamic potential Ω_0, i.e., for $(m_\Delta^2 - 4\mu^2)\Delta_0 + \frac{\lambda_\Delta}{3}\Delta_0^3 = 0$. This yields the dispersion relations

$$E_{\Delta_1}^{\pm} = \sqrt{p^2 + 4\mu^2} \pm 2\mu, \tag{33}$$

$$E_{\Delta_2}^{\pm} = \sqrt{p^2 + 4\mu^2} \pm 2\mu, \tag{34}$$

$$E_{\Delta_3}^{\pm} = \sqrt{p^2 + 12\mu^2 - m_\Delta^2 \pm \sqrt{16p^2\mu^2 + (12\mu^2 - m_\Delta^2)^2}}. \tag{35}$$

The massless NG modes in Eqs. (33) and (34) are quadratic for small momenta p, while the massless NG mode in Eq. (35) is linear for small momenta. Linear modes are referred to as type A and quadratic modes as type B. Moreover, the partners of the type-B NG modes are massive with mass 4μ.

A counting rule for the numbers of type-A and type-B NG modes has been derived in Refs. [28,29]. Denoting these numbers by n_A and n_B, respectively, the rule is

$$n_A = \dim G - \dim H - \operatorname{rank}\varrho, \tag{36}$$

$$n_B = \frac{1}{2}\operatorname{rank}\varrho, \tag{37}$$

where G is the full symmetry group, H is the unbroken subgroup, and ϱ is the commutator matrix with matrix elements

$$\varrho_{ab} = \lim_{V\to\infty}\frac{i}{V}\langle 0|[T_a, T_b]|0\rangle, \tag{38}$$

where $\langle 0|A|0\rangle$ is the ground-state expectation value of A, and V is the spatial volume of the system. It is clear that $\varrho_{ab} = 0$ if the generator T_A or T_b is unbroken. In the present case, $G = SU(3)_c$ and $H = SU(2)_c$. The only nonzero matrix elements are $\varrho_{45} = -\varrho_{54} = i\langle 0|[T_5, T_4]|0\rangle$ and $\varrho_{67} = -\varrho_{76} = i\langle 0|[T_7, T_6]|0\rangle$. This yields rank $\varrho = 4$, and therefore $n_A = 1$ and $n_B = 2$, in accordance with our explicit calculations. The commutators of the broken generators can be written as linear combination of the symmetry generators T_3 and T_8. Thus, if color charge neutrality is enforced in the 2SC phase, $Q_8 = 0$, Eq. (38) immediately yields $\varrho = 0$, and therefore the number of type-A NG bosons, n_A, equals the number of broken generators, as first shown in Ref. [33]. In the present case, a nonzero value of μ_8 breaks the $SU(3)_c$ symmetry down to $SU(2)_c \times U(1)_{Q_8}$. Diquark condensation breaks the $U(1)_{Q_8}$ symmetry, resulting in a single NG boson [25,26]. The massive modes in Eqs. (33) and (34) are also special in the sense that their gap is determined by symmetry [34]. Their number is given by the number of pairs of broken generators T_a that do not commute with T_8. There are two such pairs, $T_4 \pm iT_5$ and $T_6 \pm iT_7$, which leads to two massive NG bosons.

E. Pion condensation at finite isospin μ_I

In this section, we will discuss charged pion condensation at finite isospin chemical potential and zero baryon chemical potential. The onset of pion condensation at $T = 0$ is a

[2]The NG bosons have been discussed in the context of the NJL model in Refs. [25,26]. In the NJL model, the NG modes are propagating only after taking quark loops into account.

second-order transition that takes place exactly at the pion mass, $\mu_I = m_\pi$. As mentioned in the Introduction, QCD is amenable to lattice simulations for $\mu_B = 0$, since the sign problem is absent in this case.

Chiral perturbation theory [5,6] provides a systematic low-energy expansion of the chiral Lagrangian based on the symmetries and degrees of freedom of QCD, and gives model-independent predictions. For sufficiently small values of μ_I, we can use chiral perturbation theory to describe the BEC phase. The tree-level expressions for the pressure and the energy density in the pion-condensed phases are the same for two and three-flavor QCD, and given by [4]

$$p = \frac{1}{2} f_\pi^2 \mu_I^2 \left[1 - \frac{m_\pi^2}{\mu_I^2}\right]^2, \qquad m_\pi \leq \mu_I, \tag{39}$$

$$\epsilon(p) = -p + 2\sqrt{p(p + 2f_\pi^2 m_\pi^2)}. \tag{40}$$

In the vacuum phase, which extends from $\mu_I = 0$ to $\mu_I = m_\pi$, the pressure and energy density vanish identically, $p = \epsilon = c_s^2 = 0$. From the expressions, one can find the speed of sound squared, expressed in terms of the pion mass and the isospin chemical potential,

$$c_s^2 = \frac{dp}{d\epsilon} = \frac{\mu_I^4 - m_\pi^4}{\mu_I^4 + 3m_\pi^4}. \tag{41}$$

The speed of sound is zero in the vacuum phase and approaches unity in the ultrarelativistic limit $\mu_I \to \infty$. The large-μ_I behavior is due to the fact that the pressure is proportional to μ_I^2 and consequently the EoS becomes $\epsilon = p$ at large μ_I. However, χPT is not valid for large values of the isospin chemical potential. We can get an idea of the convergence properties of χPT at finite μ_I by comparing the predictions for different physical quantities at leading order (LO) and next to leading order (NLO). A conservative estimate suggests that χPT is reliable for μ_I up to 200 MeV [10]. The behavior at large μ_I is in disagreement with the conformal limit of QCD, where $c_s^2 = \frac{1}{3}$. The reason is that pions are not the correct degrees of freedom at high (isospin) density. In this region, one should rather think in terms of a Fermi surface that is rendered unstable due to an attractive interaction channel and the formation of loosely bound Cooper pairs of u and $\bar{d}$ quarks. Since these Cooper pairs have the same quantum numbers as the charged pions, one expects a crossover rather than a phase transition. This is called the BEC-BCS crossover. We will not focus on this crossover, but simply refer to this part of the phase diagram as the BEC/BCS phase.

The quark-meson (QM) model has also been used as a low-energy model to study QCD at finite isospin [19,35–41]. Denoting the pion condensate by ρ_0, the tree-level thermodynamic potential is

$$\Omega_0^{\mathrm{BEC/BCS}} = \frac{1}{2} m^2 \phi_0^2 + \frac{1}{2}(m^2 - \mu_I^2)\rho_0^2 + \frac{\lambda}{24}(\phi_0^2 + \rho_0^2)^2 - h\phi_0. \tag{42}$$

The one-loop thermodynamic potential with on-shell renormalization was derived in Ref. [19] for N_c colors, and we give it here for completeness,

$$\begin{aligned}\Omega_{0+1}^{\mathrm{BEC/BCS}} &= \frac{3}{4} m_\pi^2 f_\pi^2 \left\{1 - \frac{4m_q^2 N_c}{(4\pi)^2 f_\pi^2} m_\pi^2 F'(m_\pi^2)\right\} \frac{\phi_0^2 + \rho_0^2}{f_\pi^2} \\ &\quad - \frac{1}{4} m_\sigma^2 f_\pi^2 \left\{1 + \frac{4m_q^2 N_c}{(4\pi)^2 f_\pi^2} \left[\left(1 - \frac{4m_q^2}{m_\sigma^2}\right) F(m_\sigma^2) + \frac{4m_q^2}{m_\sigma^2} - F(m_\pi^2) - m_\pi^2 F'(m_\pi^2)\right]\right\} \frac{\phi_0^2 + \rho_0^2}{f_\pi^2} \\ &\quad - \frac{1}{2} \mu_I^2 f_\pi^2 \left\{1 - \frac{4m_q^2 N_c}{(4\pi)^2 f_\pi^2} \left[\log\frac{\phi_0^2 + \rho_0^2}{f_\pi^2} + F(m_\pi^2) + m_\pi^2 F'(m_\pi^2)\right]\right\} \frac{\rho_0^2}{f_\pi^2} \\ &\quad + \frac{1}{8} m_\sigma^2 f_\pi^2 \left\{1 - \frac{4m_q^2 N_c}{(4\pi)^2 f_\pi^2} \left[\frac{4m_q^2}{m_\sigma^2}\left(\log\frac{\phi_0^2 + \rho_0^2}{f_\pi^2} - \frac{3}{2}\right) - \left(1 - \frac{4m_q^2}{m_\sigma^2}\right) F(m_\sigma^2) + F(m_\pi^2) + m_\pi^2 F'(m_\pi^2)\right]\right\} \frac{(\phi_0^2 + \rho_0^2)^2}{f_\pi^4} \\ &\quad - \frac{1}{8} m_\pi^2 f_\pi^2 \left[1 - \frac{4m_q^2 N_c}{(4\pi)^2 f_\pi^2} m_\pi^2 F'(m_\pi^2)\right] \frac{(\phi_0^2 + \rho_0^2)^2}{f_\pi^4} - m_\pi^2 f_\pi^2 \left[1 - \frac{4m_q^2 N_c}{(4\pi)^2 f_\pi^2} m_\pi^2 F'(m_\pi^2)\right] \frac{\phi_0}{f_\pi} + \Omega_1^{\mathrm{fin}} + \Omega_1^{\mu},\end{aligned} \tag{43}$$

where $\rho_0^2 = \rho_{0,\overline{\mathrm{MS}}}^2$ at a reference scale, with $g_0^2\rho_0^2 = g_{0,\overline{\mathrm{MS}}}^2 \rho_{0,\overline{\mathrm{MS}}}^2$ being scale invariant, and

$$\Omega_1^{\mathrm{BECBCS,fin/BCS,fin}} = -2N_c \Lambda^{-2\epsilon} \int_p \left[E_{\rho_0}^{\pm} - 2\sqrt{p^2 + g_0^2(\phi_0^2 + \rho_0^2)} - \frac{\mu_I^2 \rho_0^2}{4[p^2 + g_0^2(\phi_0^2 + \rho_0^2)]^{\frac{3}{2}}}\right], \tag{44}$$

$$\Omega_1^{\mathrm{BEC/BCS},\mu} = 2N_c\Lambda^{-2\epsilon}\int_p [(E^\pm_{\rho_0}-\mu)\theta(\mu - E^\pm_{\rho_0}) + (E^\pm_{\rho_0}+\mu)\theta(-\mu - E^\pm_{\rho_0})]. \tag{45}$$

Here the fermionic quasiparticle spectrum is

$$E^\pm_{\rho_0} = \sqrt{\left(E \pm \frac{1}{2}\mu_I\right)^2 + g_0^2\rho_0^2}, \tag{46}$$

with $E = \sqrt{p^2 + g_0^2\phi_0^2}$. Note the similarity between the gapped spectra Eqs. (22) and (46) for $\delta\mu = 0$. The integral Eq. (44) is evaluated numerically directly in $d = 3$ dimensions. Equations (29) and (43) are the starting point for mapping out the phase diagram.

F. Behavior at large chemical potentials

For large chemical potentials μ or μ_I, we can obtain simple expressions for thermodynamic quantities such as pressure and energy density. We first consider large μ.

If we are deep in the 2SC phase, we have $\phi_0 \ll \Delta_0$. The thermodynamical potential in Eq. (29) reduces to

$$\begin{aligned}\Omega_{0+1}^{\mathrm{2SC}} &= (m^2_{\Delta,0} - 4\bar{\mu}^2)\Delta_0^2 + \frac{\lambda_{\Delta,0}}{6}\Delta_0^4 - \frac{4(4\bar{\mu}^4 + \mu_{ub}^4 + \mu_{db}^4)}{3(4\pi)^2}\\ &\quad - \frac{16 g^2_{\Delta,0}}{(4\pi)^2}\left[\log\frac{m_q^2}{g^2_{\Delta,0}\Delta_0^2} - F(m_\pi^2) - m_\pi^2 F'(m_\pi^2)\right]\bar{\mu}^2\Delta_0^2\\ &\quad + \frac{4g^4_{\Delta,0}}{(4\pi)^2}\left[\log\frac{m_q^2}{g^2_{\Delta,0}\Delta_0^2} + \frac{3}{2} - F(m_\pi^2) - m_\pi^2F'(m_\pi^2)\right]\Delta_0^4.\end{aligned} \tag{47}$$

In the same approximation, the gap equation reads

$$\begin{aligned}0 &= m^2_{\Delta,0} - 4\bar{\mu}^2 + \frac{\lambda_{\Delta,0}}{3}\Delta_0^2 - \frac{16 g^2_{\Delta,0}}{(4\pi)^2}\\ &\quad\times\left[\log\frac{m_q^2}{g^2_{\Delta,0}\Delta_0^2} - 1 - F(m_\pi^2) - m_\pi^2F'(m_\pi^2)\right]\bar{\mu}^2\\ &\quad + \frac{8 g^4_{\Delta,0}}{(4\pi)^2}\left[\log\frac{m_q^2}{g^2_{\Delta,0}\Delta_0^2} + 1 - F(m_\pi^2) - m_\pi^2F'(m_\pi^2)\right]\Delta_0^2.\end{aligned} \tag{48}$$

Assuming $\bar{\mu} \gg g_{\Delta,0}\Delta_0$, we can solve the gap equation explicitly. Denoting Δ_0 by $\bar{\Delta}_0$ in this regime, we find

$$\bar{\Delta}_0^2 = \frac{m_q^2}{g^2_{\Delta,0}}\exp\left[\frac{(4\pi)^2}{4g^2_{\Delta,0}} - 1 - F(m_\pi^2) - m_\pi^2F'(m_\pi^2)\right]. \tag{49}$$

In other words, the gap $g_{\Delta,0}\Delta_0$ approaches a constant as $\bar{\mu}\to\infty$. This is in contrast to the behavior of the gap at tree level. In this case, the gap increases linearly with $\bar{\mu}$. The difference is caused by the logarithms introduced by adding quark loops. Note that the gap $g_{\Delta,0}\bar{\Delta}_0$ depends only on the diquark coupling $g_{\Delta,0}$ and the zero-temperature quark mass m_q. In principle, we can use the result Eq. (49) to connect to perturbative QCD. We simply tune the parameter so that it agrees with the gap calculated in pQCD for a given large value of μ.[3]

The pressure p is given by minus the thermodynamic potential Ω_{0+1}, evaluated at the solution of the gap equation. At high densities, the pressure reduces to

$$p = \frac{4(4\bar{\mu}^4 + \mu_{ub}^4 + \mu_{db}^4)}{3(4\pi)^2} + \frac{16\bar{\mu}^2 g^2_{\Delta,0}\bar{\Delta}_0^2}{(4\pi)^2} + \frac{4\mu_e^4}{3(4\pi)^2}. \tag{50}$$

Except for the term $\frac{4(\mu_{sr}^4+\mu_{sg}^4+\mu_{sb}^4)}{3(4\pi)^2}$ coming from unpaired s quarks, the result for the pressure Eq. (50) is the same as obtained for the 2SC phase in the three-flavor case based on an analytic approximation of the NJL model [42].[4] The corrections to the pressure due to the color superconductivity are parametrically suppressed by $\bar{\Delta}_0^2/\bar{\mu}^2$, which can be understood as follows. Whereas Cooper pairing affects only states close to the Fermi surface, the Pauli pressure receives contributions from the entire Fermi sphere. The energy density ϵ and trace anomaly $\langle T^\alpha_{\alpha}\rangle$ are given by

$$\epsilon = \frac{4(4\bar{\mu}^4 + \mu_{ub}^4 + \mu_{db}^4)}{(4\pi)^2} + \frac{16\bar{\mu}^2 g^2_{\Delta,0}\bar{\Delta}_0^2}{(4\pi)^2} + \frac{4\mu_e^4}{(4\pi)^2}, \tag{51}$$

$$\langle T^\alpha{}_\alpha\rangle = -\frac{32\bar{\mu}^2 g^2_{\Delta,0}\bar{\Delta}_0^2}{(4\pi)^2}. \tag{52}$$

By imposing neutrality constraints, we can also obtain simple expressions for μ_e and μ_8 for very large values of μ. Expanding the thermodynamic potential around this asymptotic value and solving for the neutrality constraints Eq. (13), we arrive at the following expressions through order $\frac{1}{\mu}$

$$\begin{aligned}\mu_e &= \frac{3}{11}\left[1 + \left(\frac{9}{2}\right)^{\frac{2}{3}} - \left(\frac{9}{2}\right)^{\frac{1}{3}}\right]\mu\\ &\quad\times\left\{1 + \frac{2}{9}\left[1 + \left(\frac{2}{9}\right)^{\frac{1}{3}}\right]\frac{g^2_{\Delta,0}\bar{\Delta}_0^2}{\mu^2}\right\}\\ &\approx 0.57\mu\left[1 + 0.36\frac{g^2_{\Delta,0}\bar{\Delta}_0^2}{\mu^2}\right],\end{aligned} \tag{53}$$

[3] We have to multiply by $2^{-\frac{1}{3}}$ since the CFL gap is related to the 2SC gap by this factor [2].

[4] The chemical potentials μ_{sr}, μ_{sg}, and μ_{sb} are expressed in terms of μ, μ_e, μ_8 as well as the mass m_s of the s quark.

$$\mu_8 = \frac{9}{11}\left[1-\left(\frac{375}{32}\right)^{\frac{1}{3}}+\left(\frac{125}{48}\right)^{\frac{1}{3}}\right]\mu \times\left\{1-\frac{50}{27}\left[1+\left(\frac{162}{125}\right)^{\frac{1}{3}}+\left(\frac{4}{3}\right)^{\frac{1}{3}}\right]\frac{g_{\Delta,0}^2\bar{\Delta}_0^2}{\mu^2}\right\} \approx 0.09\mu\left[1-5.91\frac{g_{\Delta,0}^2\bar{\Delta}_0^2}{\mu^2}\right]. \tag{54}$$

It is interesting to note that both chemical potentials μ_e and μ_8 are independent of the gap at asymptotic values of the quark chemical potential and therefore grow linearly with μ. This is in contrast to the 2SC phase with three flavors [42]. The pressure p receives the extra contribution from the unpaired s quarks as explained below Eq. (50). The extra contributions to the neutrality equations from this term cancel the leading-order contributions in Eqs. (53) and (54) (for $m_s = 0$) so that μ_e and μ_8 are both of order $\frac{\bar{\Delta}_0^2}{\mu}$. Inserting the expansions Eqs. (53) and (54) into the expressions for the pressure Eq. (50) and energy density Eq. (51), we obtain the speed of sound for neutral matter at large μ

$$c_s^2 = \frac{1}{3}\left\{1+\frac{4}{9}\left[1+\left(\frac{2}{9}\right)^{\frac{1}{3}}\right]\frac{g_{\Delta,0}^2\bar{\Delta}^2}{\mu^2}\right\} \approx \frac{1}{3}\left[1+0.71\frac{g_{\Delta,0}^2\bar{\Delta}_0^2}{\mu^2}\right]. \tag{55}$$

In this form, it is easy to see that the speed of sound approaches the conformal limit from above. In the case $\mu_e = \mu_8 = 0$, the coefficient of the correction term is $\frac{2}{3}$ [18]. Thus, the speed of sound relaxes faster to $c_s = \frac{1}{\sqrt{3}}$ if charge neutrality is not imposed. Imposing neutrality, these simple relations hold as long as we can safely ignore the last term in (31). This can be done as long as $\delta\mu \geq g_{\Delta,0}\Delta_0$. We found in (53) that μ_e grows linearly with μ. This implies that at some later stage, for larger chemical potential, this term becomes relevant. The effect on the system is that it is energetically beneficial for a smaller diquark gap and one would see a decrease to smaller or zero value on Δ_0.

Comparing Eqs. (29) and (43), we note that the expressions for the thermodynamic potential are essentially the same, the one-loop terms differ by numerical factors and the relevant couplings. This implies that the gap, pressure, energy density, trace anomaly, and speed of sound have the same behavior at large μ_I. As in the 2SC phase, we calculate the thermodynamic potential deep into the BCS phase using $\phi_0 \approx 0$. This yields

$$\bar{\rho}_0^2 = \frac{m_q^2}{g_0^2}\exp\left[\frac{(4\pi)^2}{4N_c g_0^2} - 1 - F(m_\pi^2) - m_\pi^2 F'(m_\pi^2)\right], \tag{56}$$

$$p = \frac{N_c\mu_I^4}{6(4\pi)^2} + \frac{2N_c\mu_I^2 g_0^2\bar{\rho}_0^2}{(4\pi)^2}, \tag{57}$$

$$\epsilon = \frac{N_c\mu_I^4}{2(4\pi)^2} + \frac{2N_c\mu_I^2 g_0^2\bar{\rho}_0^2}{(4\pi)^2}, \tag{58}$$

$$\langle T^{\alpha}{}_{\alpha}\rangle = -\frac{4N_c\mu_I^2 g_0^2\bar{\rho}_0^2}{(4\pi)^2}, \tag{59}$$

$$c_s^2 = \frac{1}{3}\left[1+\frac{4g_0^2\bar{\rho}_0^2}{\mu_I^2}\right]. \tag{60}$$

In contrast to the superconducting gap, the asymptotic value of the pion condensate $\bar{\rho}_0$ is completely determined by vacuum physics.

III. RESULTS AND DISCUSSION

In this section, we discuss our numerical results. The values of the meson masses and the pion decay constant are

$$m_\pi = 140\ \text{MeV}, \tag{61}$$

$$m_\sigma = 600\ \text{MeV}, \tag{62}$$

$$f_\pi = 93\ \text{MeV}. \tag{63}$$

In addition, the quark mass is

$$m_q = 300\ \text{MeV}. \tag{64}$$

We also set $N_c = 3$. As we have explained, the remaining parameters are treated as free. A natural guess for the parameters would be $g_\Delta \sim g$, $\lambda \sim \lambda_3 \sim \lambda_\Delta$, which in [18] was shown to yield reasonable results. It turns out that the results are sensitive mainly to the diquark mass parameter m_Δ and the diquark coupling g_Δ. The position of the transition to the 2SC phase depends on both parameters, while the gap is largely determined by the latter. For asymptotically large values of μ, the gap depends only on $\bar{\Delta}_0$ (in addition to the quark and pion mass).

To illustrate the possible phase diagrams, we have chosen two sets of parameters Table II, The first set is one of the four parameter sets used in our previous analysis in Ref. [18]. The second set was chosen to show that NQM is possible when neutrality has been imposed (see Fig. 4 below). We mentioned in Sec. II F that we can determine g_Δ by equating our asymptotic value for the gap to the gap at large densities obtained from pQCD. We can also determine it from other constraints on the gap at large densities.

TABLE II. Parameter values for the two sets of parameters.

…	m_Δ	g_Δ	λ_3	λ_Δ
Set 1	500 MeV	$2g$	λ	$\frac{1}{4}\lambda$
Set 2	900 MeV	$\frac{3}{2}g$	λ	$\frac{1}{4}\lambda$

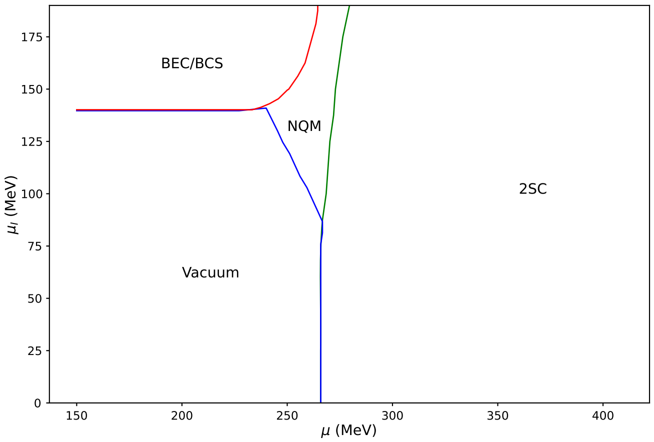

FIG. 1. Phase diagram in the μ–μ_I plane at $T = 0$ for parameters set 1. See main text for details.

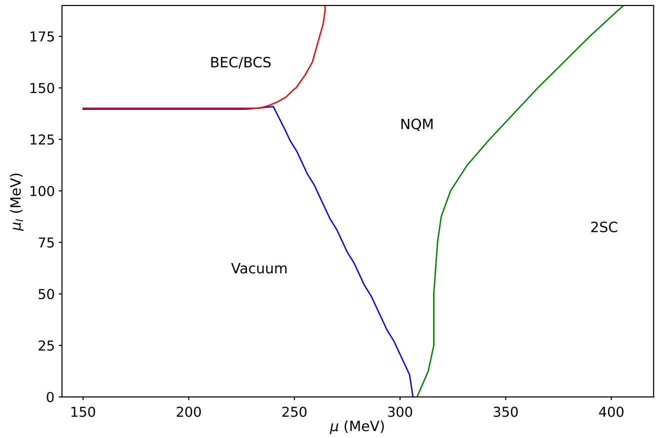

FIG. 2. Phase diagram in the μ–μ_I plane at $T = 0$ for parameters set 2. See main text for details.

Recently, [43] used astrophysical observations to obtain an upper bound on the CFL gap of 216 MeV at baryon chemical potential $\mu_B = 2.6$ GeV. We therefore ensure that our gap for the first set does not exceed this limit $g_\Delta \Delta_0 \leq 268 = 2^{-\frac{1}{3}}216$ MeV for large μ,while the gap for set two we allow to go beyond. More generally, the parameter with the largest effect is g_Δ. Increasing g_Δ leads to an earlier transition from vacuum or NQM to the 2SC phase. Increasing g_Δ also leads to lower gap values in our analysis. Lastly, increasing (decreasing) m_Δ leads to a later (earlier) transition to the 2SC phase, either from the vacuum or NQM. Constraining these parameters is therefore most important. To find the minimum of the thermodynamic potential Ω_{0+1}, we must simultaneously solve the two gap equations

$$\frac{\partial \Omega_{0+1}^{2SC}}{\partial \phi_0} = \frac{\partial \Omega_{0+1}^{2SC}}{\partial \Delta_0} = 0, \qquad (2SC), \tag{65}$$

$$\frac{\partial \Omega_{0+1}^{BEC/BCS}}{\partial \phi_0} = \frac{\partial \Omega_{0+1}^{BEC/BCS}}{\partial \rho_0} = 0, \qquad (BEC/BCS) \tag{66}$$

using Eqs. (29) and (43), respectively. For given values of μ and μ_I, we compare Ω_{0+1}^{2SC} and $\Omega_{0+1}^{BEC/BCS}$ and then choose the global minimum. Imposing electric charge and color charge neutrality in the 2SC phase, the Eqs. (13) and (65) are solved simultaneously. The neutrality constraints reduces the number of independent chemical potential from three to one, for example μ. The quark condensate and the superconducting gap, as well as μ_e and μ_8 are then functions of μ.

In Fig. 1, we show the zero-temperature phase diagram in the μ–μ_I plane using parameter set 1. The red line is the phase boundary between the pion-condensed phase and the vacuum phase or normal quark matter. The blue line is the phase boundary between the vacuum phase and either normal quark matter or the 2SC phase, whereas the green line is the phase boundary between NQM and the color superconducting phase.

In Fig. 2, we show the zero-temperature phase diagram in the μ–μ_I plane using parameter set 2. The color coding is the same as in Fig. 1, but now normal quark matter exists in a much larger region in the plane. Below we shall see that this gives rise to electrically neutral normal quark matter.

In Fig. 3, we show the quark condensate (black line), the superconducting gap (green line), the electron chemical potential μ_e (blue line), and the color chemical potential μ_8 (red line) as functions of the quark chemical potential μ for parameter set 1. For these parameters, the transition is directly from the vacuum to the 2SC phase. The chemical potentials μ_e and μ_8 vanish in the entire region up to the transition to the 2SC phase, reflecting that the vacuum state is neutral. Since the 2SC ground state carries both color and electric charge, both chemical potentials μ_e and μ_8 are nonzero in order to satisfy the charge neutrality conditions.

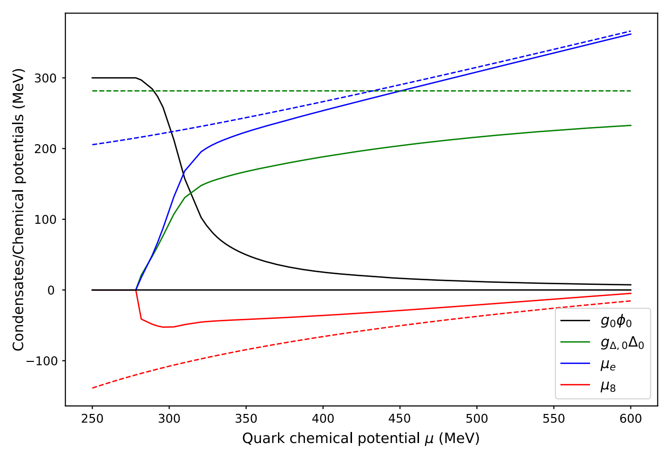

FIG. 3. Quark condensate (black line), superconducting gap (green line), electron chemical potential (blue line), and color chemical potential (red line) as functions of μ for parameter set 1. See main text for details.

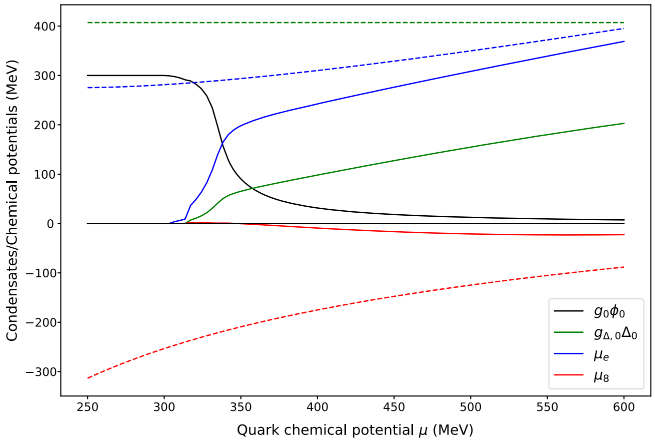

FIG. 4. Quark condensate (black line), superconducting gap (green line), electron chemical potential (blue line), and color chemical potential (red line) as functions of μ for parameter set 2. See main text for details.

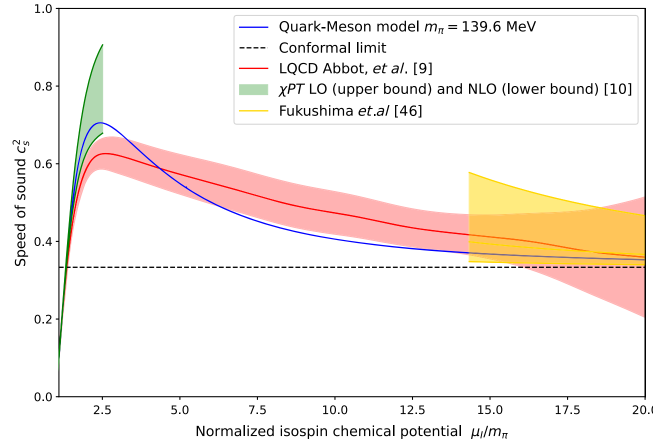

FIG. 6. Speed of sound squared in the pion-condensed phase versus μ_I/m_π. See main text for details.

Note that $\mu_e > 0$ such that the electron density is positive, which is needed to neutralize the positively charged 2SC state. The superconducting gap approaches a constant for large values of the chemical potential μ, cf. Eq. (49). Similarly, the large-μ behaviors of μ_e and μ_8 are given by Eqs. (53) and (54). These equations are shown as dashed lines in the figure, green for the asymptotic behavior of the gap, blue for μ_e, and red for μ_8. The behavior of the gap is in contrast to the behavior in the NJL model regulated by a conventional three-dimensional cutoff Λ, where the gap has a maximum at $\mu \approx 500$ MeV, after which it drops rather quickly to zero. As pointed out in Ref. [44], this unphysical behavior is a regularization artifact. However, in recent work on the NJL model using renormalization group ideas [45], this problem is absent.

In Fig. 4, we show the same quantities as in Fig. 3, but now for parameter set 2. The difference is that there is a phase of normal quark matter between the vacuum phase and the 2SC phase. Two-flavor normal quark matter is not

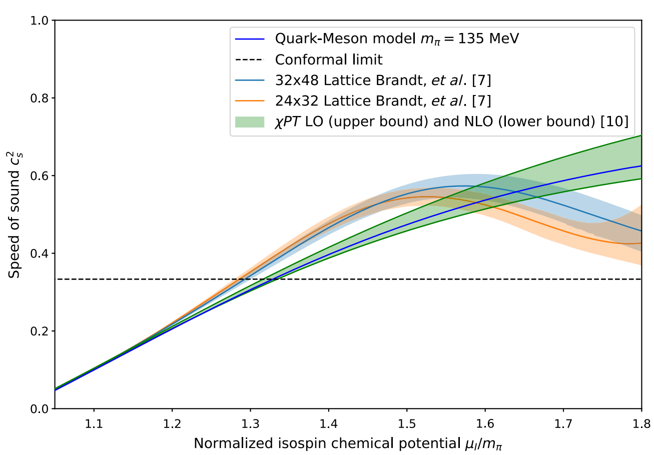

FIG. 5. Speed of sound squared in the pion-condensed phase versus μ_I/m_π. See main text for details.

electrically neutral without an electron background, which is why $\delta\mu = \frac{1}{2}\mu_e$ (blue line) becomes nonzero before the superconducting gap (green line) and μ_8 (red line). Note that the red lines in Figs. 3 and 4 eventually cross the x axis, so μ_8 becomes positive for sufficiently large values of μ, which is in agreement with large-μ behavior given by (54).

Next, we consider the speed of sound, which is of interest because it gives information about the stiffness of the EoS. The EoS is crucial in understanding the structure of neutron stars. Before we discuss the case of finite quark chemical potential, we consider finite isospin for which lattice data exist. For similar results and analyses, see Ref. [38] and very recently Ref. [41]. In Fig. 5, we show the result for the speed of sound squared c_s^2 as a function of μ_I/m_π using the quark-meson model (blue line). We also show the results for two-flavor chiral perturbation theory [10] to leading order and next-to-leading order. The green band is simply the region between the LO (upper line) and the NLO (lower line) results. Note that the blue curve lies entirely within this band. We also show the results of lattice simulations using two different lattices [7], given by the light blue and yellow bands. In the lattice simulations, $m_\pi = 135$ MeV and $f_\pi = 90$ MeV were used. In this range of isospin chemical potentials, χPT and the quark-meson model are in good qualitative agreement with the lattice data, although the peak in c_s^2 occurs much earlier than in the QM model (See Fig. 6).

In Fig. 6, we show the result for the speed of sound squared c_s^2 using the QM model for a wide range of values for μ_I/m_π (blue line). The green band is the χPT result [10] obtained as explained above. The red band is the result of the lattice simulations of Ref. [9] with $m_\pi = 139.6$ MeV and $f_\pi = 92$ MeV. The band was constructed from 2000 bootstrap samples with $\pm$ two standard deviations from the mean. The yellow band is the result of the calculations in Ref. [46]. The authors calculated the speed of sound, and trace anomaly using the Cornwall-Jackiw-Tomboulis

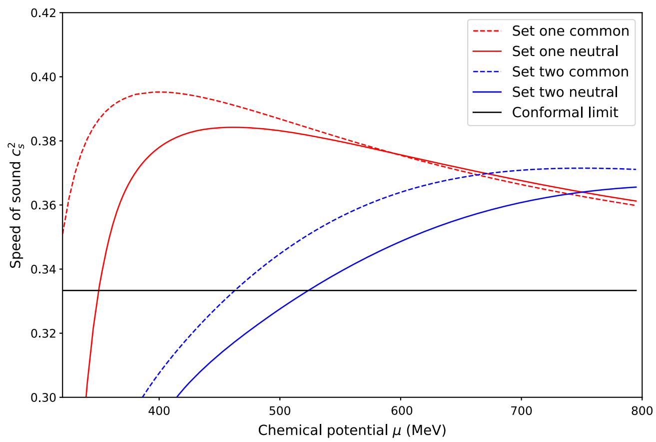

FIG. 7. Speed of sound squared in the 2SC phase for parameter set 1 (red) and set 2 (blue) versus μ. Dashed lines are without charge neutrality and solid lines are with charge neutrality. See main text for details.

formalism [47], including the gap in their two-loop calculations. Their band is obtained by varying the renormalization scale $\Lambda = X\mu$ with $X = 1$ to $X = 3$. Our results show that c_s^2 increases sharply from the onset of pion condensation at $\mu_I = m_\pi$ with a peak at $\mu_I \approx 335$ MeV. After the peak, the speed of sound relaxes to the conformal limit (shown as the black dashed line). As pointed out in Ref. [41], the overall good agreement with lattice data over a wide range of isospin densities is remarkable. It is also in qualitative agreement with the perturbative calculation of [46].

In Fig. 7, we show the speed of sound squared c_s^2 as a function of the quark chemical potential. The red lines correspond to dataset 1 and the blue lines refer to dataset 2. Dashed lines are without electric and color charge neutrality, and solid lines are with. Moreover, the peak of c_s^2 moves to higher values of μ, and the peak is also lower. Thus, requiring charge neutrality softens the EoS. We emphasize that this property and the relaxation to the conformal limit from above are generic features of the QMD model. From Eq. (55) and the remarks below it, it follows that c_s with neutrality constraints imposed is larger than c_s without charge neutrality, for sufficiently large values of μ. This is the case for parameter set 1, as can be seen in Fig. 7. We have checked that the blue curves are crossing each other for larger values of μ.

Regarding the structure of c_s, we must be cautious, since our calculations are for two flavors. Extending our calculations to three flavors, we except to find a CFL phase for large μ. If the transition from the 2SC phase to the CFL phase is first order, the speed of sound will be discontinuous. Thus, we will not make a detailed comparison with other approaches [48]. That being said, a peak of c_s^2 has also been found in quarkyonic matter [49]. On the other hand, the perturbative treatment of [46] discussed above predicts that the conformal limit is approached from below. Finally, the peak in the speed of sound is particularly interesting in view of recent neutron star observations. Using agnostic approaches, Refs. [50,51] find a peak, whereas Ref. [52] observes a plateau, as the baryon density increases. It is possible to confront QMD model calculations with observation. Combining mass-radius measurements of neutron stars with Bayesian inference [53,54], it is possible to find the probability distributions of its parameters.

Since we are interested in applying the QMD model to compact stars, we briefly discuss different possibilities for hybrid stars, i.e., stars with a core of deconfined quarks. In a compact star, a possible scenario is several phase transitions as we increase the baryon density. The first transition is from hadronic matter to normal quark matter. The second transition is from normal quark matter to a color superconducting phase. Whether this transition is to the 2SC phase or directly to the CFL depends on the details of the models (masses and couplings) and is an open question. One can ask the question whether the transition is sharp or it is via a mixed phase. A sharp transition takes place at a specific value for the quark chemical potential at which the pressures of the two phases are equal. In each phase, neutrality constraints are imposed locally. The existence of a mixed phase requires a first-order transition between the two phases. In such a two-component system, neutrality constraints are imposed globally [55]. This means that the system is overall neutral with respect to the relevant conserved charges, but one component is positively charged and the other is negatively charged. Following Ref. [56], we consider the possibility of a mixed phase of normal quark matter and 2SC matter. Since normal quark matter is neutral with respect to the color charge Q_8, we also impose $\frac{\partial \Omega_{0+1}}{\partial \mu_8} = 0$ on the 2SC phase. If the density in the core of the star is not too high, it is possible that it contains a mixture of normal quark matter and 2SC matter, that is, a nonstrange hybrid star is realized. If the density in the core is sufficiently high, one expects a transition to the CFL phase, so we need to extend the QMD model to three flavors. Work in these directions is in progress [57].

Note added. In the final stages of this work, Ref. [41] appeared. Their analysis of the pion-condensed phase and comparison with lattice simulations are similar to ours.

ACKNOWLEDGMENTS

The authors thank B. Brandt *et al.* [7], R. Abbott *et al.* [9], and K. Fukushima [46] for permission to use their lattice data. J. O. A. also thanks B. Brandt, G. Endrodi, and L. von Smekal for useful discussions.

DATA AVAILABILITY

The data that support the findings of this article are openly available [58].

[1] K. Rajagopal and F. Wilczek, *At the Frontier of Particle Physics* (World Scientific, Singapore, 2001), Vol. 3, p. 2061.
[2] M. G. Alford, A. Schmitt, K. Rajagopal, and T. Schäfer, Rev. Mod. Phys. **80**, 1455 (2008).
[3] K. Fukushima and T. Hatsuda, Rep. Prog. Phys. **74**, 014001 (2011).
[4] D. T. Son and M. A. Stephanov, Phys. Rev. Lett. **86**, 592 (2001).
[5] J. Gasser and H. Leutwyler, Ann. Phys. (N.Y.) **158**, 142 (1984).
[6] J. Gasser and H. Leutwyler, Nucl. Phys. **B250**, 465 (1985).
[7] B. B. Brandt, F. Cuteri, and G. Endrodi, J. High Energy Phys. 07 (2023) 055.
[8] R. Abbott, W. Detmold, F. Romero-López, Z. Davoudi, M. Illa, A. Parreño, R. J. Perry, P. E. Shanahan, and M. L. Wagman (NPLQCD Collaboration), Phys. Rev. D **108**, 114506 (2023).
[9] R. Abbott, W. Detmold, M. Illa, A. Parreño, R. J. Perry, F. Romero-López, P. E. Shanahan, and M. L. Wagman, Phys. Rev. Lett. **134**, 011903 (2025).
[10] J. O. Andersen, M. K. Johnsrud, Q. Yu, and H. Zhou, Phys. Rev. D **111**, 034017 (2025).
[11] P. F. Bedaque and T. Schäfer, Nucl. Phys. **A697**, 802 (2002).
[12] M. Alford and K. Rajagopal, J. High Energy Phys. 06 (2002) 031.
[13] S. B. Rüster, V. Werth, M. Buballa, I. A. Shovkovy, and D. H. Rischke, Phys. Rev. D **72**, 034004 (2005).
[14] H. Abuki and T. Kunihiro, Nucl. Phys. **A768**, 118 (2006).
[15] T. Gorda, A. Kurkela, P. Romatschke, S. Säppi, and A. Vuorinen, Phys. Rev. Lett. **121**, 202701 (2018).
[16] T. Gorda, R. Paatelainen, S. Säppi, and K. Seppänen, Phys. Rev. Lett. **131**, 181902 (2023).
[17] L. Fernandez and J.-L. Kneur, Phys. Rev. Lett. **129**, 212001 (2022); Phys. Rev. D **111**, 034020 (2025).
[18] J. O. Andersen and M. P. Nødtvedt, Phys. Rev. D **111**, 034031 (2025).
[19] J. O. Andersen and P. Kneschke, Phys. Rev. D **97**, 076005 (2018).
[20] I. A. Shovkovy, Found. Phys. **35**, 1309 (2005).
[21] A. Gerhold and A. Rebhan, Phys. Rev. D **68**, 011502 (2003).
[22] D. D. Dietrich and D. H. Rischke, Prog. Part. Nucl. Phys. **53**, 305 (2004).
[23] I. A. Shovkovy and M. Huang, Phys. Lett. B **564**, 205 (2003).
[24] R. Casalbuoni, Z. Duan, and F. Sannino, Phys. Rev. D **62**, 094004 (2000).
[25] D. Blaschke, D. Ebert, K. G. Klimenko, M. K. Volkov, and V. L. Yudichev, Phys. Rev. D **70**, 014006 (2004).
[26] D. Ebert, K. G. Klimenko, and V. L. Yudichev, Phys. Rev. D **72**, 056007 (2004).
[27] H. B. Nielsen and S. Chadha, Nucl. Phys. **B105**, 445 (1976).
[28] H. Watanabe and H. Murayama, Phys. Rev. Lett. **108**, 251602 (2012).
[29] Y. Hidaka, Phys. Rev. Lett. **110**, 091601 (2013).
[30] A. Nicolis, R. Penco, F. Piazza, and R. A. Rosen, J. High Energy Phys. 11 (2013) 055.
[31] H. Watanabe, T. Brauner, and H. Murayama, Phys. Rev. Lett. **111**, 021601 (2013).
[32] T. Brauner, *Effective Field Theory for Spontaneously Broken Symmetry*, Lecture Notes Physics Vol. 1023 (Springer Verlag, Berlin, 2024).
[33] T. Schäfer, D. T. Son, and M. A. Stephanov, D. Toublan, and J. J. M. Verbaarschot, Phys. Lett. B **522**, 67 (2001).
[34] A. Nicolis and F. Piazza, Phys. Rev. Lett. **110**, 011602 (2013),**110**, 039901(A) (2013).
[35] L.-Y. He, M. Jin, and P.-F. Zhuang, Phys. Rev. D **71**, 116001 (2005).
[36] K. Kamikado, N. Strodthoff, L. von Smekal, and J. Wambach, Phys. Lett. B **718**, 1044 (2013).
[37] A. Ayala, A. Bandyopadhyay, R. L. S. Farias, L. A. Hernández, and J. L. Hernández, Phys. Rev. D **107**, 074027 (2023).
[38] R. Chiba and T. Kojo, Phys. Rev. D **109**, 076006 (2024).
[39] A. Ayala, B. S. Lopes, R. L. S. Farias, and L. C. Parra, Phys. Lett. B **864**, 139396 (2025).
[40] J. P. Carlomagno, D. G. Dumm, and N. N. Scoccola, Phys. Rev. D **109**, 094041 (2024).
[41] B. B. Brandt, V. Chelnokov, G. Endrodi, G. Marko, D. Scheid, and L. von Smekal, Phys. Rev. D **112**, 054038 (2025).
[42] A. W. Steiner, S. Reddy, and M. Prakash, Phys. Rev. D **66**, 094007 (2002).
[43] A. Kurkela, K. Rajagopal, and R. Steinhorst, Phys. Rev. Lett. **132**, 262701 (2024).
[44] M. Huang, P.-F. Zhuang, and W.-Q. Chao, Phys. Rev. D **67**, 065015 (2003).
[45] H. Gholami, M. Hofmann, and M. Buballa, Phys. Rev. D **111**, 014006 (2025).
[46] K. Fukushima and S. Minato, Phys. Rev. D **111**, 094006 (2025).
[47] J. M. Cornwall, R. Jackiw, and E. Tomboulis, Phys. Rev. D **10**, 2428 (1974).
[48] G. Baym, T. Hatsuda, T. Kojo, P. D. Powell, Y. Song, and T. Takatsuka, Rep. Prog. Phys. **81**, 056902 (2018).
[49] L. McLerran and S. Reddy, Phys. Rev. Lett. **122**, 122701 (2019).
[50] S. Altiparmak, C. Ecker, and L. Rezzolla, Astrophys. J. Lett. **939**, L34 (2022).
[51] M. Marczenko, L. McLerran, K. Redlich, and C. Sasaki, Phys. Rev. C **107**, 025802 (2023).
[52] L. Brandes, W. Weise, and N. Kaiser, Phys. Rev. D **108**, 094014 (2023).
[53] M. Albino, T. Malik, M. Ferreira, and C. Providência, Phys. Rev. D **110**, 083037 (2024).
[54] A. Ayriyan, D. Blaschke, J. P. Carlomagno, G. A. Contrera, and A. G. Grunfeld, Universe **11**, 141 (2025).
[55] N. K. Glendenning, Phys. Rev. D **46**, 1274 (1992).
[56] I. A. Shovkovy, M. Hanauske, and M. Huang, Phys. Rev. D **67**, 103004 (2003).
[57] J. O. Andersen and M. P. Nødtvedt (to be published).
[58] https://github.com/mathiaspno/2FQMDmodel/tree/main.